Chemical Science

ROYAL SOCIETY OF CHEMISTRY

EDGE ARTICLE

View Article Online
View Journal | View Issue

Check for updates

Cite this: *Chem. Sci.*, 2024, **15**, 16291

All publication charges for this article have been paid for by the Royal Society of Chemistry

Received 23rd May 2024
Accepted 12th September 2024

DOI: 10.1039/d4sc03387f

rsc.li/chemical-science

Open Access Article. Published on 12 September 2024. Downloaded on 2/22/2026 8:42:32 PM. This article is licensed under a Creative Commons Attribution-NonCommercial 3.0 Unported Licence.

Fluorescence-plane polarization for the real-time monitoring of transferase migration in living cells†

Yafu Wang,[a] Huiyu Niu,[a] Kui Wang,[a] Liu Yang,[a] Ge Wang,[d] Tony D. James, [ac] Jiangli Fan *[b] and Hua Zhang *[a]

Transferases are enzymes that exhibit multisite migration characteristics. Significantly, enzyme activity undergoes changes during this migration process, which inevitably impacts the physiological function of living organisms and can even lead to related malignant diseases. However, research in this field has been severely hindered by the lack of tools for the simultaneous and differential monitoring of site-specific transferase activity. Herein, we propose a novel strategy that integrates a fluorescence signal response with high sensitivity and an optical rotation signal response with superior spatial resolution. To validate the feasibility of this strategy, transferase γ-glutamyltransferase (GGT) was used as a model system to develop dual-mode chiral probes **ACx-GGTB** (**AC17-GGTB** and **AC15-GGTB**) using chiral amino acids as specific bifunctional recognition groups. The probes undergo structural changes under GGT, resulting in the release of bifunctional recognition groups (chiral amino acids) and simultaneously generate fluorescence signals and optical rotation signals. This dual-mode output exhibits high sensitivity and facilitates differentiation of sites. Furthermore, it enables simultaneous and differential detection of GGT activity at different sites during migration. We anticipate that probes developed based on this strategy will facilitate imaging-based monitoring of the activity for other transferases, thus providing an imaging platform suitable for the real-time tracking of transferase activity changes during migration.

Introduction

Transferases can facilitate the transfer of various functional groups from one substrate to another. These enzymes include transmethylase (*e.g.*, glutathione S-transferase),[1] transaminase (*e.g.*, γ-glutamyltransferase, GGT),[2] hexokinase (*e.g.*, glycosyltransferase),[3] phosphorylase,[4] and so on. The catalytic transfer function of transferases is crucial for numerous essential physiological processes in cells and organisms.[1–6] For example, GGT plays a pivotal role in glutathione metabolism and homeostasis.[7–9] It exhibits widespread distribution across various cellular organelles and serves as a significant clinical marker for hepatobiliary diseases.[10,11] Another characteristic feature of transferases is their ability to undergo multisite migration within cells, ultimately localizing at a different site from the site of generation. For example, GGT is synthesized and processed in the endoplasmic reticulum (ER) before being translocated to the cytomembrane.[12] This property is ubiquitous among most transferases. Thus, alterations in transferase activity at different sites during metastasis, from the initial generation site to the final aggregation site, have profound implications for various physiological functions and ultimately contribute to malignant diseases.[13,14] Monitoring these dynamic changes in activity across different locations represents an important frontier in transferase research. However, the rapid fluctuations in transferase activity and occurrence of numerous cellular reactions are a significant challenge for the monitoring of enzyme activity during migration.

At present, most of the reported probes for monitoring enzyme activity at a cellular single-site (such as the mitochondria, ER and cell membrane) rely on fluorescence response mode,[15–34] for example, a photo-crosslinking probe with high resolution for nitroreductase at the mitochondria,[15] a highly sensitive fluorescent probe for carboxylesterase-2 at the ER,[16] and a solid-state luminescent probe for GGT at the cell membrane.[17] However, there are currently no reported fluorescent probes capable of the real-time monitoring of transferase activity along the migration pathway with high spatial resolution at multiple sites.[35] Therefore, how to optimize the high spatial resolution of fluorescent probes and construct a new

[a]*Collaborative Innovation Centre of Henan Province for Green Manufacturing of Fine Chemicals, Key Laboratory of Green Chemical Media and Reactions, Ministry of Education, Henan Key Laboratory of Organic Functional Molecule and Drug Innovation, School of Chemistry and Chemical Engineering, Henan Normal University, Xinxiang, Henan 453007, P. R. China. E-mail: zhh1106@htu.edu.cn; Fax: +86-373-3329030; Tel: +86-373-3329030*

[b]*State Key Laboratory of Fine Chemicals, Frontiers Science Center for Smart Materials, Oriented Chemical Engineering, School of Chemical Engineering, Dalian University of Technology, Dalian, Liaoning 116024, P. R. China. E-mail: fanjl@dlut.edu.cn*

[c]*Department of Chemistry, University of Bath, Bath, BA2 7AY, UK*

[d]*Xinxiang Medical University, Xinxiang 453000, P. R. China*

† Electronic supplementary information (ESI) available. See DOI: https://doi.org/10.1039/d4sc03387f

© 2024 The Author(s). Published by the Royal Society of Chemistry

Open Access Article. Published on 12 September 2024. Downloaded on 2/22/2026 8:42:32 PM.
This article is licensed under a Creative Commons Attribution-NonCommercial 3.0 Unported Licence.

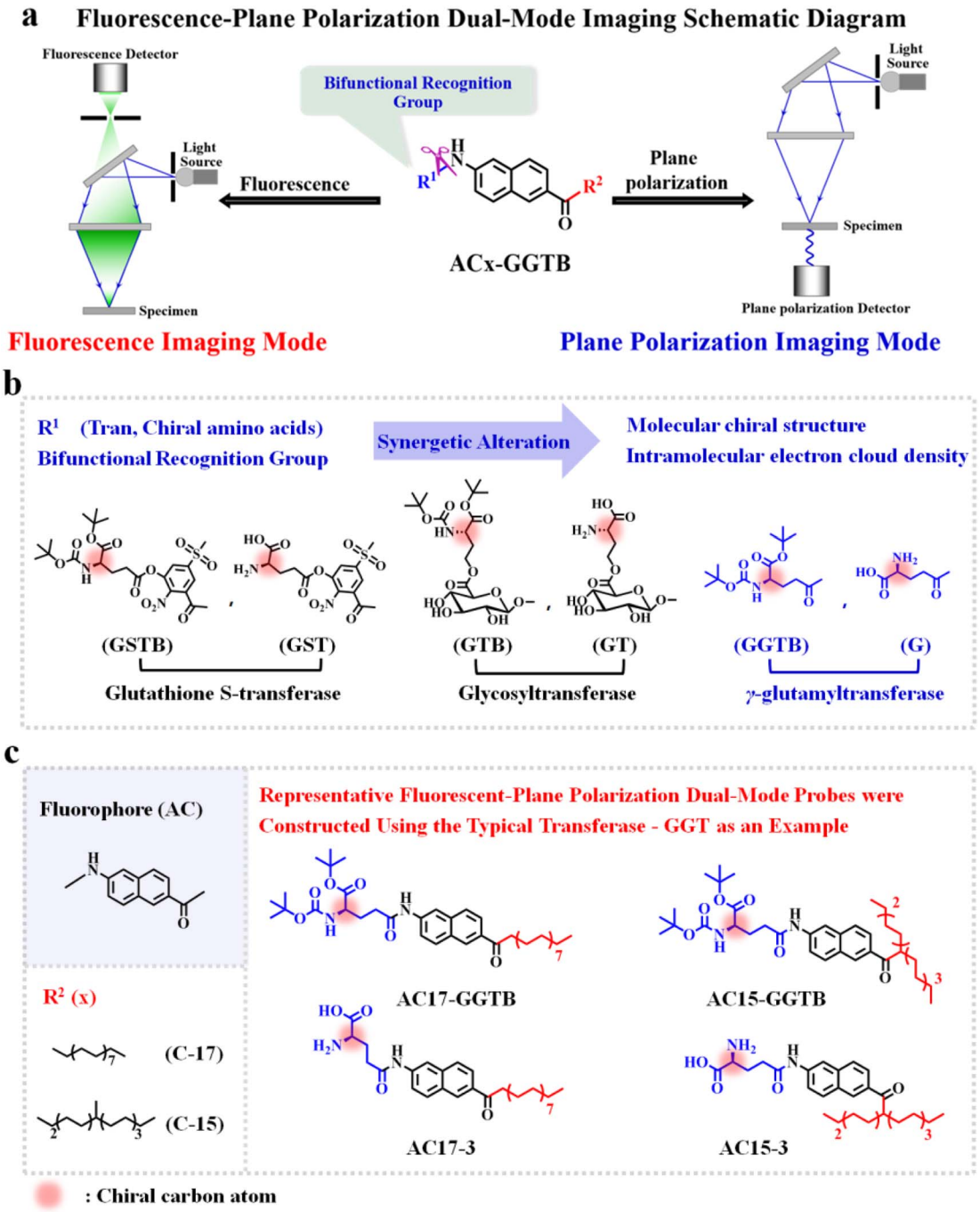

Fig. 1 (a) Schematic for fluorescence-plane polarization dual-mode imaging and the corresponding molecular skeleton of chiral probes. (b) Bifunctional recognition groups for different kinds of transferases (R^1). They are chiral amino acids and named Tran. Among them, GSTB and GST for glutathione S-transferase, GTB and GT for glycosyltransferase, GGTB and G for γ-glutamyltransferase. (c) Fluorescent-plane polarization dual-mode probes for typical transferase-GGT. AC, fluorophore. R^2, alkyl chain groups to adjust the water–oil amphiphilicity of the probes. The red glows indicate the chiral carbon atom.

method for monitoring multi-site transferase activity is the focus and difficulty of this work.

Molecular chirality can induce plane polarization and exhibit optical rotation signals.[36] Thus, plane polarization microimaging can be used to monitor biomacromolecules in real-time at multiple sites with high spatial resolution.[37,38] This property might make up for the shortcomings in the fluorescence imaging of transferase activity based on the above traditional fluorescent probes. And in many cases the inherent optical rotation of biomolecules such as collagen can be monitored. Alternatively, optical rotation signals from biological stains such as chiral (hematoxylin) or non-chiral (eosin) have been used to monitor the chiral biomolecules.[39–41] And the binding of fluorescently tagged drugs with protein targets has

© 2024 The Author(s). Published by the Royal Society of Chemistry

Open Access Article. Published on 12 September 2024. Downloaded on 2/22/2026 8:42:32 PM.
This article is licensed under a Creative Commons Attribution-NonCommercial 3.0 Unported Licence.

been monitored using changes in optical rotation.[42] These mean that the chiral probes based on plane polarization imaging technology are expected to monitor the multi-site transferase activity in living cells with high spatial resolution. However, a limitation of plane polarization imaging is its low sensitivity. Therefore, we propose a novel design strategy (Fig. 1a) for transferase probes by introducing chiral recognition groups (Fig. 1b) at one end of the probes as recognition groups to simultaneously activate the changes in both highly sensitive fluorescence and high spatial resolution optical rotation. We anticipate that this strategy would address the limitations associated with using just fluorescence or plane polarization imaging methods.

Results and discussion

Probe design

To validate the feasibility of this design strategy, GGT was selected as a typical representative example due to its diverse intracellular metastatic properties and high expression levels during various tumorigenesis processes (*e.g.*, hepatoma, oophoroma and colorectal carcinoma). We have designed and synthesized a series of molecules (**AC*x*-GGTB**, Fig. 1) capable of emitting fluorescence-plane polarization dual-mode signals. In molecular design, we chose [6-acetyl-2-methylaminonaphthalene] (Aceman, AC) as the fluorophore (Fig. 1) which exhibits significant fluorescence sensitivity due to intramolecular charge transfer (ICT). In order to achieve the simultaneous fluorescence and optical rotation signal response, chiral bifunctional recognition groups *N*-boc-L-glutamate 1-*tert*-butyl ester (GGTB) and L-glutamate (G) for GGT (R^1, Fig. 1b) were introduced into **AC*x*-GGTB**, whose dissociation can activate simultaneous alterations in the molecular chiral structure and intramolecular electron cloud density. The alkyl chain groups (R^2, Fig. 1c) are important for regulating water–oil amphiphilicity,[43] thereby enhancing the ability to traverse organelles possessing different membrane structures, such as the ER, cell membrane and so on. It is anticipated that this kind of molecules will exhibit differentiated fluorescence and optical rotation signal responses, which can be attributed to the formation of a range of hydrolysates during the enzymatic reaction with GGT in living cells.

Fluorescence and optical rotation signal changes in PBS

Taking **AC17-GGTB** as an example, the changes in fluorescence and optical rotation under the action of GGT were verified. A weak blue fluorescence signal was observed at 422 nm (Fig. 2a, $\Phi_{\mathbf{AC17\text{-}GGTB}} = 0.07$, $\tau_{\mathbf{AC17\text{-}GGTB}} = 2.6$ ns) under 325 nm excitation in the absence of enzymes (Fig. S1†) in PBS (pH = 7.4). However, the absorbance and fluorescence signals exhibited an increase (Fig. 2, S1 and S2†) when **AC17-GGTB** reacts with GGT. This was primarily attributed to the conversion of **AC17-GGTB** to AC17 (Fig. 3, $\Phi_{AC17} = 0.21$, $\tau_{AC17} = 2.8$ ns), whose structural changes were also monitored. And the fluorescence intensities of other intermediate products (AC17-1a, AC17-1b, AC17-2 and AC17-3, Fig. 3) are similar to that of **AC17-GGTB** ($\Phi_{\mathbf{AC17\text{-}GGTB}} = 0.07$, $\Phi_{AC17\text{-}3} = 0.10$) during the reaction of **AC17-GGTB** with GGT, which is due to that the bifunctional recognition group GGTB has not been fully removed, therefore, still inhibiting the fluorescence. A good linear correlation was observed between GGT activity (0–0.78 U mL^{-1}) and fluorescence signal intensity at 422 nm for **AC17-GGTB** ($I_{422nm} = 3.7 \times 10^5 + 6.1 \times 10^5$ C_{GGT}, Fig. 2b). The minimum detection limit of **AC17-GGTB** for GGT activity was determined to be 1.78×10^{-3} U mL^{-1}. Furthermore, the response time is rapid within 1.0 s (Fig. 2c and d), which is advantageous for monitoring GGT activity during its transfer from the generation site to the final aggregation site in living cells. In addition, under the same conditions (PBS, pH = 7.4), the fluorescence signal of **AC17-GGTB** at 422 nm remained unchanged for 4.0 h, which ruled out the existence of self-aggregation or dissociation of the probe to affect the detection of GGT activity (Fig. S1e†). And the observed fluorescence response was only observed in the presence of GGT, while other coexisting compounds in the cells, including biological macromolecules, ions and amino acids exhibited negligible effect on the fluorescence signal (Fig. S3†). These results can be attributed to the specific cleavage by GGT that targets the amide bond of **AC17-GGTB** ($m/z_{[M+Li+H]}$: 701.4934), resulting in the production of AC17 ($m/z_{[M+NH_4-3H]}$: 424.8876) and GGTB ($m/z_{[M+2H]}$: 305.1486, Fig. S4†). In addition, to further confirm the

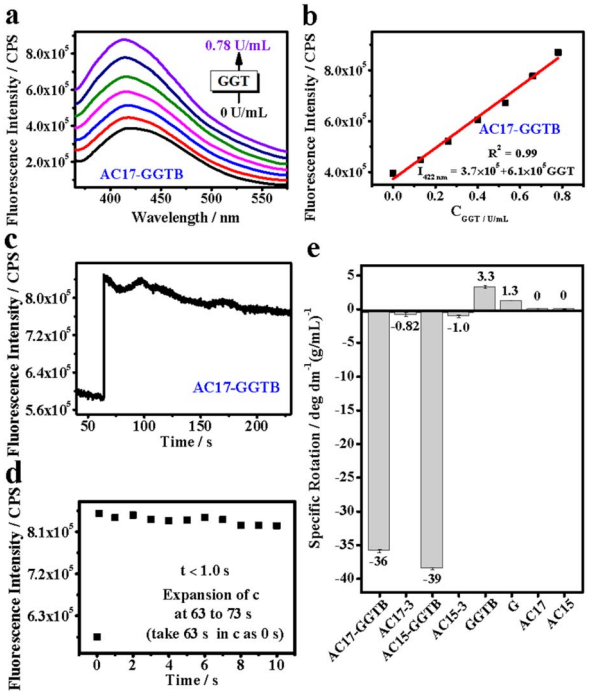

Fig. 2 Response of AC*x*-GGTB (15 μM) for GGT activity in PBS (pH = 7.4). (a) Emission spectrum of **AC17-GGTB** for GGT activity (0–0.78 U mL^{-1}, λ_{ex} = 325 nm). (b) Linear response of **AC17-GGTB** for GGT activity in the emission spectrum (a) ($I_{422nm} = 3.7 \times 10^5 + 6.1 \times 10^5$ GGT (R^2 = 0.99)). (c) Dynamic response of **AC17-GGTB** for GGT activity (0.39 U mL^{-1}). (d) Local expansion of (c) (63 s in (c) was taken as 0 s). (e) Specific rotation ($[\alpha]_{\lambda t}$) of AC*x*-GGTB (1.5 g/100 mL) and its metabolites (1.5 g/100 mL) at 25 °C in dichloromethane. Data are representative of replicate experiments (n = 5).

Open Access Article. Published on 12 September 2024. Downloaded on 2/22/2026 8:42:32 PM. This article is licensed under a Creative Commons Attribution-NonCommercial 3.0 Unported Licence.

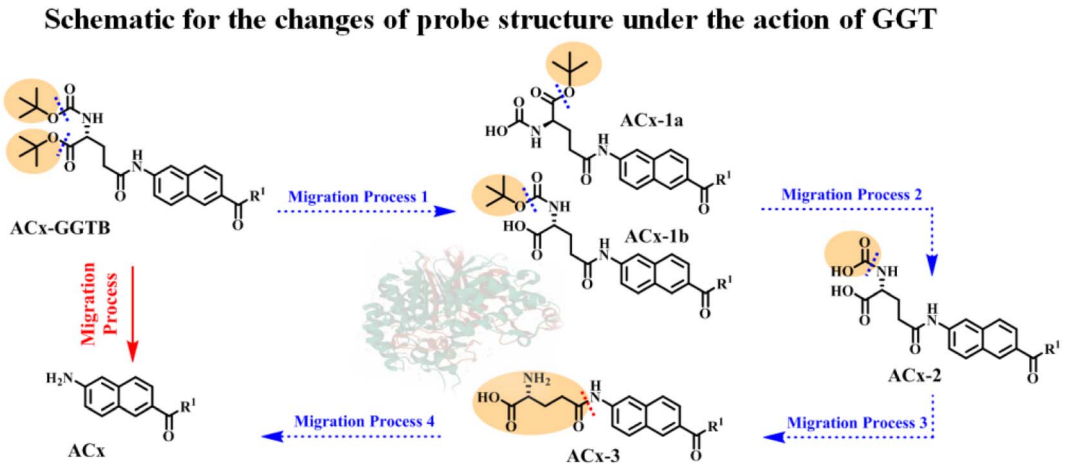

Fig. 3 Changes of probe structure under the action of GGT.

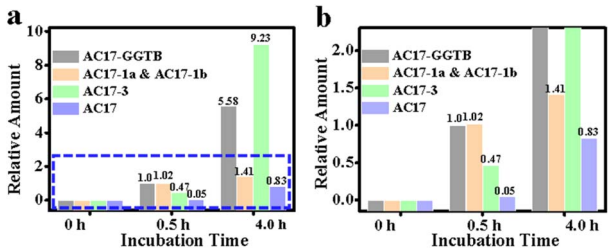

Fig. 4 LC-MS/MS analysis of the transfer and recognition process of AC17-GGTB in living HepG2 cells. a, LC-MS/MS analysis of the migration and recognition process of AC17-GGTB in cells. (b) Expansion of the blue area of (a). Incubation concentration: 20 μM. Incubation time: 0.5 h, 4.0 h.

above spectral response results, similar commercial molecules A (1-(6-amino-2-naphthyl)ethanone) and B (*N*-(6-acetyl-2-naphthalenyl)acetamide) were used as controls to test the change of photophysical properties in different solvents (Fig. S5, S6 and Table S1†). The photophysical properties of **AC17-GGTB**, AC17 and control molecules (A, B) were found to be almost identical in solutions other than PBS (pH = 7.4). However, in PBS, the wavelengths of **AC17-GGTB** and AC17 were obviously blue-shifted, and the fluorescence signal intensity was significantly reduced. These phenomena, combined with related reports,[43] were attributed to the introduction of the longer alkyl chain ($C_{17}H_{35}$) within **AC17-GGTB**. Moreover, it was also confirmed that the fluorescence signal of **AC17-GGTB** in PBS (pH = 7.4) was linearly enhanced with the increase of concentration (2–12 μM), which again excluded the occurrence of aggregation affecting its fluorescence signal, and verified the spectral response results of **AC17-GGTB** to GGT above (Fig. S7†). And we also verified that **AC15-GGTB** possesses similar fluorescence recognition performance for GGT activity (Fig. S1, S2, S3, and S8†). Therefore, **ACx-GGTB** was suitable for the sensitive fluorescence detection of GGT activity.

When there is a change in the fluorescence signal, it simultaneously generates an optical rotation signal change, both of which are correlated with GGT activity. The specific rotation ($[\alpha]_{\lambda t}$) value for **AC17-GGTB** was −35.86 (Fig. 2e). However, the

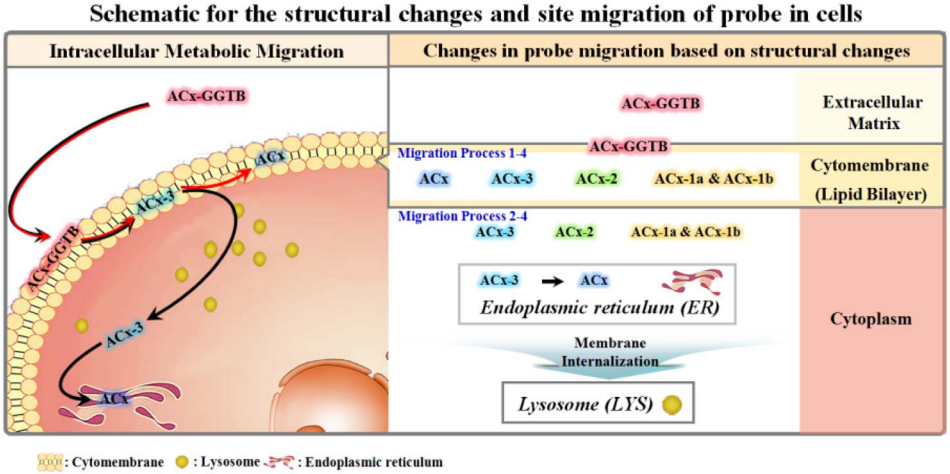

Fig. 5 Schematic for the structural changes and site migration of the probe in cells. The structure of the probes changes gradually in the cell, which leads to the transfer from the cytomembrane to the ER.

© 2024 The Author(s). Published by the Royal Society of Chemistry

Open Access Article. Published on 12 September 2024. Downloaded on 2/22/2026 8:42:32 PM.
This article is licensed under a Creative Commons Attribution-NonCommercial 3.0 Unported Licence.

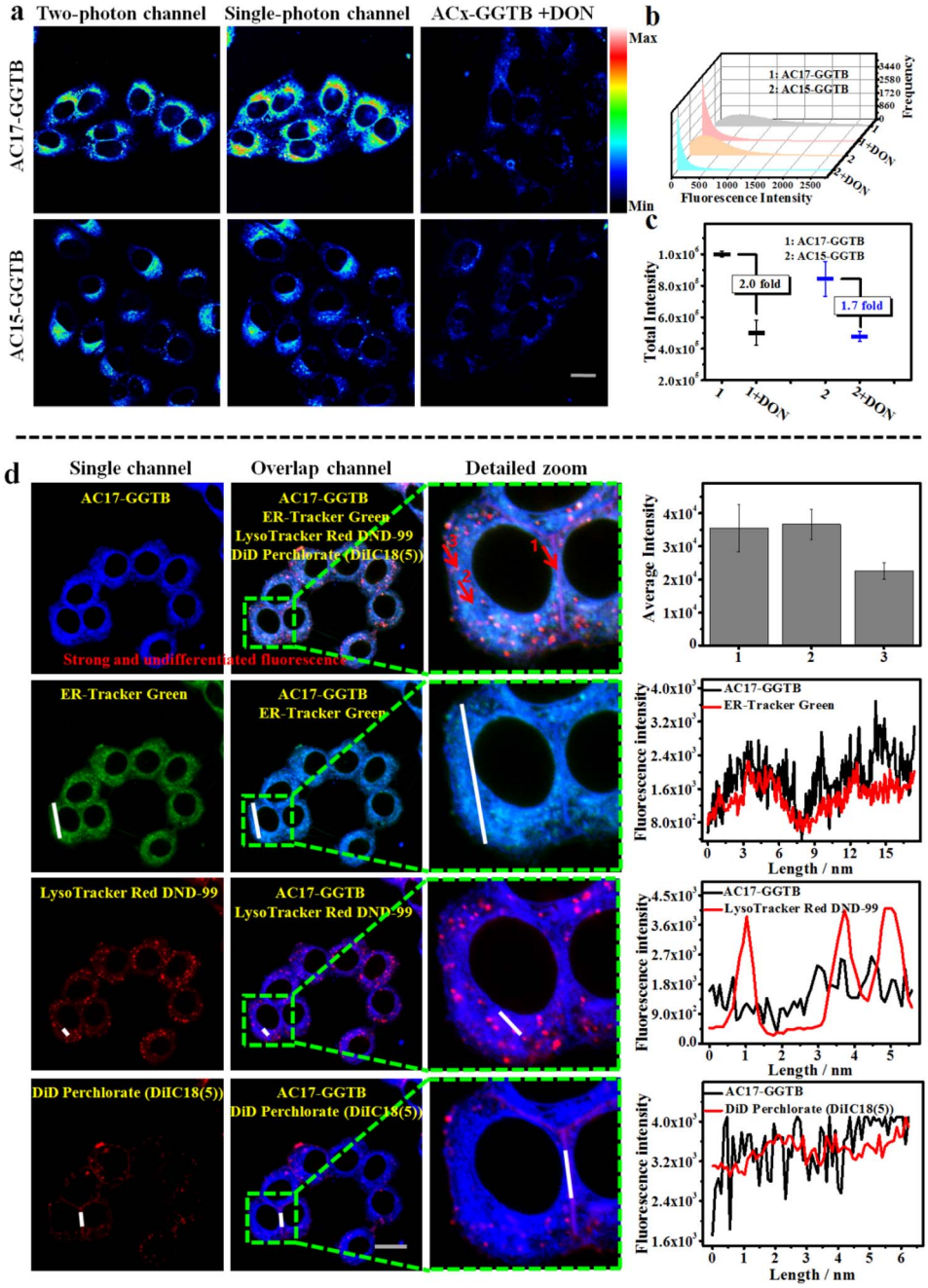

Fig. 6 Fluorescence imaging of **AC17-GGTB** in HepG2 cells. (a) One/two-photon fluorescence imaging in HepG2 cells. Single-photon excitation wavelength = 405 nm, two-photon excitation wavelength = 800 nm, scan range = 420–460 nm. Incubation concentration: 20 μM. Incubation time: 3.0 h. **ACx-GGTB** + DON: the cells were first incubated with the inhibitor DON (1.0 mM) for 1.0 h, and then incubated with the **ACx-GGTB** (20 μM) for 3.0 h. (b) The high throughput date statistics of the blue channel in the two-photon channel. 1, **AC17-GGTB**; 2, **AC15-GGTB**. (c) The total intensity data in the two-photon channel. (d) Colocalization imaging of **AC17-GGTB** in HepG2 cells. **AC17-GGTB**: incubation time: 3.0 h, excitation wavelength = 405 nm, scan range = 420–460 nm (Blue Channel); ER-Tracker Green: endoplasmic reticulum commercial probe, incubation time: 0.5 h, excitation wavelength = 488 nm, scan range = 505–555 nm (Green Channel); LysoTracker Red DND-99: lysosome commercial probe, incubation time: 0.5 h, excitation wavelength = 559 nm, scan range = 580–630 nm (Red Channel); DiD Perchlorate (DiIC18(5)): cell membrane commercial probe, incubation time: 0.5 h, excitation wavelength = 635 nm, scan range = 650–700 nm (Red Channel). Overlay Channel: fitting diagram of the four channels. Internal PMTs are at 16 bit and 1600 × 1600 pixels, and scan speed is 400 Hz. Scan: 10 μm.

amide bond within the probes is cleaved upon encountering GGT. Consequently, **AC17-GGTB** is converted to achiral AC17, resulting in the loss of optical activity. The $[\alpha]_{\lambda t}$ values for the metabolites **AC17-3**, AC17, BOC-L-glutamate-1-*tert*-butyl ester, and L-glutamate are −0.82, 0, 3.27, and 1.25, respectively. These experimental results confirm that the probe enables the detection of GGT activity exploiting differences in optical rotation signals mediated by GGT activity.

© 2024 The Author(s). Published by the Royal Society of Chemistry

Open Access Article. Published on 12 September 2024. Downloaded on 2/22/2026 8:42:32 PM. This article is licensed under a Creative Commons Attribution-NonCommercial 3.0 Unported Licence.

Fluorescence and optical rotation signal changes and response mechanism at multiple sites of living cells

The fluorescence and optical rotation response signal changes originate from the structural changes of **AC17-GGTB** under the action of GGT directly. That is, the response mechanism at multiple sites of living cells was first verified in this section. As such, the molecular changes of chiral probe **AC17-GGTB** (20 μM) were assessed in living cells using a Liquid Chromatography-QExactive Mass Spectrometer (LC-MS/MS, Fig. 4). **AC17-GGTB** and its metabolites exhibited high stability (photostability, Fig. S9;† pH stability, Fig. S10†), appropriate water solubility (Fig. S11†), and low cytotoxicity towards living cells (Fig. S12†). Fig. 4 confirmed the presence of **AC17-GGTB** and its metabolites in both experimental groups at different incubation times (0.5 and 4.0 h), with the levels increasing over time (Fig. 4 and S11†). Furthermore, the content of **AC17-GGTB** at 0.5 h was considered as the baseline, while the relative amounts of **AC17-GGTB**, and metabolites AC17-1a/b, AC17-3, and AC17 in cells at 4.0 h were found to be 5.58, 1.41, 9.23, and 0.83, respectively. This indicated that there are multiple structural changes of the probe during the recognition process with GGT in living cells.

We then used quantitative structure–activity relationships[44] (QSAR) to verify alterations in the intracellular localization of **AC17-GGTB** with specific structural changes during GGT migration, utilizing the electric charge (Z), the amphiphilicity index (AI) and the logarithm of the octanol–water partition coefficient ($\log P$) as evaluation parameters. The analysis results revealed (Fig. 5) that **AC17-GGTB** (AI = 7.13, $\log P = 7.82$) could efficiently localize in the cytomembrane ($5 < \mathrm{AI} < 8$, $5 < \log P < 8$). Subsequently, **AC17-GGTB** was sequentially transesterated into primary esterolysis intermediates (AC17-1a and/or AC17-1b) and secondary esterification products (AC17-2, $\log P = 5.33$) in the complex environment of the cytoplasm, which could be localized in the cytomembrane and cytoplasm ($0 < \log P < 6$). Then AC17-2 was further rapidly decomposed into the amino acid derivative AC17-3 (AI = 4.22, $\log P = 5.08$, which could be protonated to form an ammonium salt with $Z > 0$) with the help of the cellular microenvironment. It could diffuse to the cytomembrane and ER ($3.5 < \mathrm{AI} < 6$, $0 < \log P < 6$, $Z > 0$) and simultaneously react with GGT activity *in situ* to form AC17. The QSAR analyses provide preliminary evidence supporting the localization of **AC17-GGTB** and its metabolites at different sites in living cells.

We further investigated the intracellular fluorescence and optical rotation signals in the recognition process of GGT using cell imaging. Fig. 6a confirmed a highly sensitive fluorescence signal at 420–460 nm towards GGT activity, which was achieved by one-photon (405 nm) or two-photon (800 nm) excitation in living HepG2 cells when incubated with **AC17-GGTB** (20.0 μM). The undifferentiated fluorescence signal of **AC17-GGTB** and its metabolites (AC17-3 and AC17) also supported this finding within the cells (Fig. S14 and S15†). Furthermore, the addition of 1.0 mM of DON (a typical GGT inhibitor) during pretreatment resulted in reduced fluorescence signal intensities that were significantly lower than those observed for untreated cells (Fig. 6b and c). Additionally, differences in the fluorescence signal intensity between different sites within the cells were further observed (Fig. 6d, Marker 1: cytomembrane; Marker 2: ER; Marker 3: lysosome). The detected fluorescence signal intensity was strong and sensitive but did not differentiate between the different sites involved in GGT migration, *i.e.* Markers 1, 2, and 3.

To further prove the differentiation of signals at different sites, the optical rotation signal was determined in living model cells with inhibited GGT activity. As shown in Fig. 7, **AC17-GGTB**

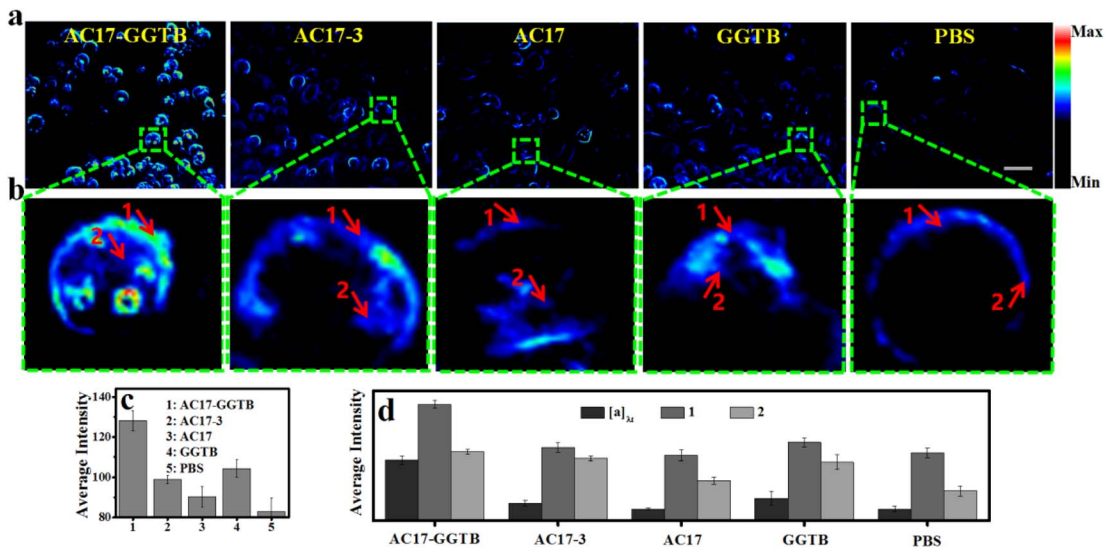

Fig. 7 Plane polarization imaging in model cells. (a) Plane polarization imaging of probe AC17-GGTB and the enzyme metabolites and PBS (pH = 7.4, control) in model cells. (b) The expansion of the green area in (a). (c) Optical rotation signal intensity data statistics in (a). (d) Optical rotation signal intensity data statistics of the marked sites in (b). $[\alpha]_{\lambda t}$, optical activity of the probe and its metabolites; 1, 2, markers in (b). Incubation concentration: 20 μM. Incubation time: 3.0 h. Scan: 50 mm.

© 2024 The Author(s). Published by the Royal Society of Chemistry

Open Access Article. Published on 12 September 2024. Downloaded on 2/22/2026 8:42:32 PM.
This article is licensed under a Creative Commons Attribution-NonCommercial 3.0 Unported Licence.

exhibited an enhance optical rotation signal within the cytomembrane region (Marker 1), which was significantly stronger than other areas (Fig. 7b and d). Intermediate metabolites such as AC17-3 and GGTB could simultaneously exist in both the cytomembrane and cytoplasm, while AC17-3 also exhibited a certain amount of penetration into the ER. Although the molecules exhibit certain optical rotation activity, their relatively dispersed distribution within the cell resulted in comparable signal intensities between the plasma membrane (Marker 1) and other areas (Marker 2). Meanwhile, the overall optical rotation signal of AC17, the final product of GGT enzymatic hydrolysis, is significantly weaker than that of **AC17-GGTB** due to nonchiral AC17 lacking inherent optical rotation activity, as such the optical rotation signals originate from the target site-cytomembrane or ER. However, there is a significant increase in the signal intensity of AC17 in the cytomembrane region (Marker 1) compared to the ER region (Marker 2), facilitated by differences between these two regions. Additionally, cells incubated with **AC17-GGTB** exhibit a significantly stronger optical rotation signal intensity compared to the control group, further confirming that **AC*x*-GGTB** can monitor the GGT activity at different target sites within cells using plane polarization imaging based on changes in optical rotation activity before and after recognition by GGT at various cellular locations. Therefore, combining highly sensitive fluorescence with region-specific optical rotation enables differential monitoring of GGT activity along the migration pathways within cells using **AC*x*-GGTB**. Moreover, more significantly, the same polarizing imaging results were obtained in living tissues (Fig. S16†).

Fluorescence-plane polarization dual mode monitoring of GGT metabolism in living cells

The normal physiological metabolism model in HepG2 cells was established to further verify the applicability of fluorescence-plane polarization dual-mode imaging probes for the monitoring of GGT activity between different sites. HepG2 cells were incubated with **AC17-GGTB** for various times (10, 30, 60, 90, and 120 min), and simultaneous detection using the dual-mode imaging signals was performed. Fig. 8 indicates a minimal fluorescence signal throughout the cytomembrane

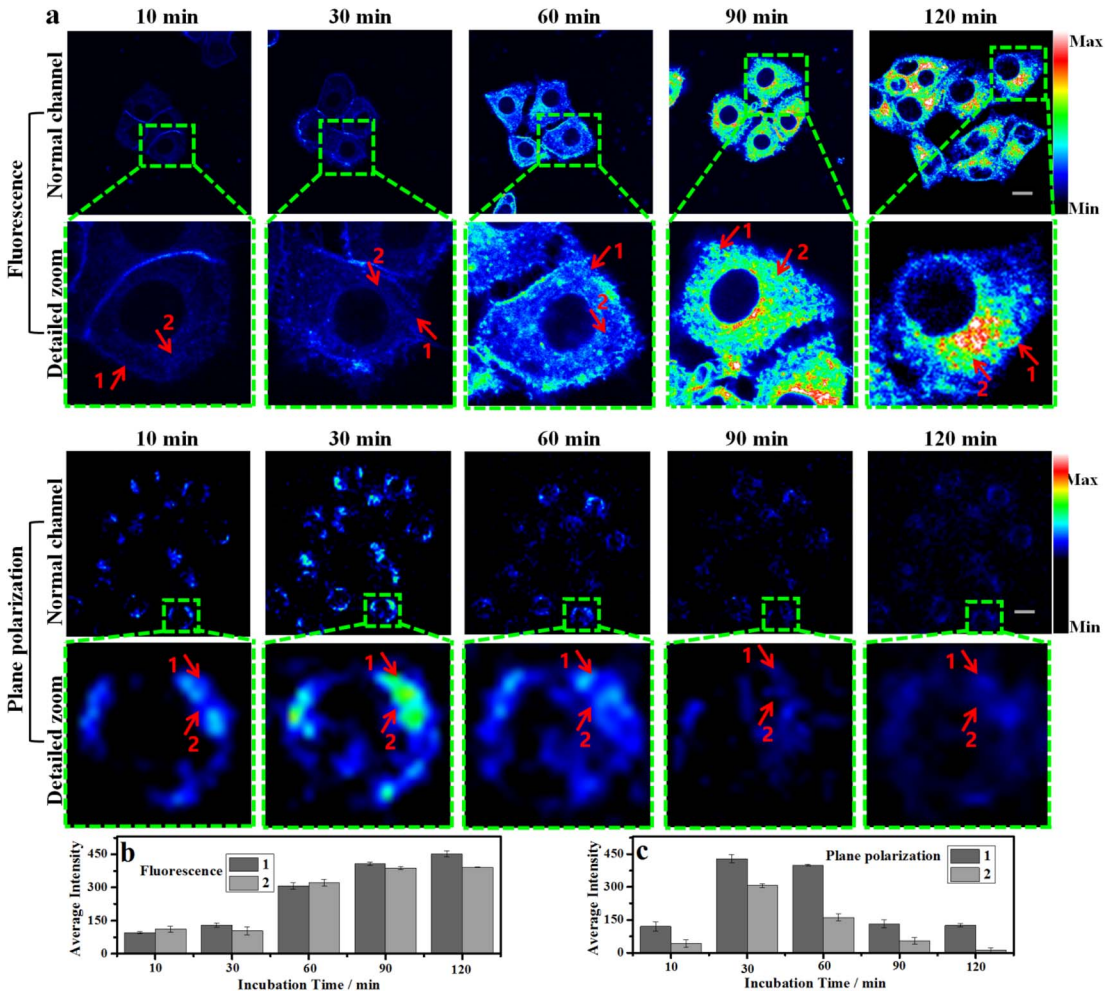

Fig. 8 Fluorescence-plane polarization dual-mode imaging in HepG2 cells. (a) Fluorescence plane polarization dual-mode imaging of AC17-GGTB for GGT activity in HepG2 cells. (b) and (c) The fluorescence (b) and optical rotation (c) signal intensity data statistics of the marker sites in (a). Two-photon excitation wavelength = 800 nm, scan range = 420–460 nm (blue channel). Incubation concentration: 20 μM. Scan in fluorescence imaging: 10 μm. Scan in polarization imaging: 10 mm.

Open Access Article. Published on 12 September 2024. Downloaded on 2/22/2026 8:42:32 PM. This article is licensed under a Creative Commons Attribution-NonCommercial 3.0 Unported Licence.

after 30 min incubation. Conversely, a pronounced optical rotation signal was observed. As the incubation time increased, there was a significant enhancement in the fluorescence signal. Then, after an incubation period of 120 min, a strong yet indistinguishable fluorescence signal was observed (Fig. 8a and b), accompanied by a significant decrease in the optical rotation signal (Fig. 8a and c). However, it should be noted that the optical rotation signal inside the cell remained consistently lower than that at the cytomembrane (Markers 1 and 2 in plane polarization of Fig. 8a and c). This result was attributed to variations in GGT activity between the different sites. Moreover, the fluorescence signal remained consistent between the two sites upon exposure to GGT at both the cytomembrane and ER (Markers 1 and 2 in fluorescence of Fig. 8a and b at 90 min and 120 min). However, a significantly stronger optical rotation signal was observed at the cytomembrane compared to that at the ER (Fig. 8a and c) due to disparities in the metabolites' optical activity. These findings validate the ability of the **AC17-GGTB** probes to selectively monitor GGT activity at multiple sites during migration. The above experimental results confirmed the feasibility of this design strategy for detecting transferases in living cells, provided that the molecular structure incorporates essential functional groups, namely fluorescence-plane polarization bifunctional recognition groups (*e.g.*, (*R*)-5-(3-acetyl-5-(methylsulfonyl)-2-nitrophenoxy)-2-amino-5-oxopentanoic acid and *O*-((2*S*,3*S*,4*S*,5*R*,6*R*)-3,4,5-trihydroxy-6-methoxytetrahydro-2*H*-pyran-2-carbonyl)-L-homoserine) as well as flexible hydrophobic groups (*e.g.*, *n*-octane, hexylene diamine, and 3-(*tert*-butyl-amino) butyric acid). As such a dual-mode fluorescent-plane polarization probe was constructed that exhibits highly sensitive fluorescence and high spatiotemporal resolution of the optical rotation signals and can be used to monitor the activity of transferases in living cells.

Conclusions

Fluorescence-plane polarization dual-mode imaging chiral probes were developed to monitor changes in transferase activity between different sites during migration in living cells. In order to validate the design concept, **AC*x*-GGTB** was used as an illustrative example to monitor GGT activity at multiple intracellular sites. QSAR model analysis and LC-MS/MS analysis confirmed that the probes could undergo structural modification and transfer between distinct locations in response to the enzymatic action of GGT. Spectroscopic and imaging results further corroborated the capability of **AC*x*-GGTB** for the dual-mode monitoring of GGT activity using fluorescence-plane polarization during intracellular migration in living cells. As such our research confirms the feasibility of the current design strategy and highlights the potential utility of fluorescence-plane polarization dual-mode imaging probes for investigating transferase activity, as well as diagnosing and treating related diseases.

Data availability

The data supporting this article have been included as part of the ESI.†

Author contributions

Y. F. W., J. L. F. and H. Z. proposed the concept and supervised the work; Y. F. W., T. D. J., J. L. F. and H. Z. designed the experiments and wrote the paper; Y. F. W., T. D. J., J. L. F. and H. Z. contributed to the discussion and provided suggestions. Y. F. W., H. Y. N., G. W., L. Y., and H. Z. helped to analyse the data; Y. L. helped with the theoretical calculation and related data analysis; Y. F. W., K. W., and H. Z. helped to summarize the data. All authors have discussed the results, drafted the manuscript and approved the final version of the manuscript.

Conflicts of interest

There are no conflicts to declare.

Acknowledgements

This work was supported by the National Natural Science Foundation of China (U21A20314, 21925802, 22107089, and 52271251); the Program for Innovative Research Team in Science and Technology in University of Henan Province (23IRTSTHN002); T. D. J. wishes to thank the Royal Society for a Wolfson Research Merit Award and the Open Research Fund of the School of Chemistry and Chemical Engineering, Henan Normal University for support (2020ZD01). T. D. J has been appointed as an Outstanding Talent by Henan Normal University.

Notes and references

1 E. Abdelraheem, B. Thair, R. F. Varela, E. Jockmann, D. Popadić, H. C. Hailes, J. M. Ward, A. M. Iribarren, E. S. Lewkowicz, J. N. Andexer, P. L. Hagedoorn and U. Hanefeld, *ChemBioChem*, 2022, **23**(18), e202200212.
2 K. Zakharia, S. J. Klair and R. A. Murali, *Dig. Dis.*, 2019, **37**(6), 518.
3 R. S. Carolina, E. M. M. Luis, B. P. Andrés, K. D. Beatriz, L. C. Montserrat and S. N. Sobeida, *Front. Mol. Biosci.*, 2021, **8**, 701975.
4 L. Nagy, J. Márton, A. Vida, G. Kis, É. Bokor, S. Kun, M. Gönczi, T. Docsa, A. Tóth, M. Antal, P. Gergely, B. Csóka, P. Pacher, L. Somsák and P. Bai, *Br. J. Pharmacol.*, 2018, **175**, 301.
5 J. Shekhawat, K. Gauba, S. Gupta, B. Choudhury, P. Purohit, P. Sharma and M. Banerjee, *J. Cancer Res. Clin.*, 2021, **147**, 1869.
6 T. Kasahara, T. C. Chang, H. Yoshioka, S. Urano, Y. Egawa, M. Inoue, T. Tahara, K. Morimoto, A. R. Pradipta and K. Tanaka, *Chem. Sci.*, 2024, **15**, 9566.
7 Y. Ogawa, H. Hosoyama, M. Hamano and H. Motai, *Agric. Biol. Chem.*, 1991, **55**(12), 2971.
8 S. S. Tate and A. Meister, *Mol. Cell. Biochem.*, 1981, **39**(1), 357.
9 G. A. Thompson and A. Meister, *J. Biol. Chem.*, 1977, **252**(19), 6792.
10 V. I. Kulinsky and L. S. Kolesnichenko, *Biochem. Mosc. Suppl. S*, 2009, **3**(3), 211.

© 2024 The Author(s). Published by the Royal Society of Chemistry

Open Access Article. Published on 12 September 2024. Downloaded on 2/22/2026 8:42:32 PM. This article is licensed under a Creative Commons Attribution-NonCommercial 3.0 Unported Licence.

11 M. H. Hanigan and H. C. Pitot, *Carcinogenesis*, 1985, **6**(2), 165.
12 C. L. Kinlough, P. A. Poland, J. B. Bruns and R. P. Hughey, *Methods Enzymol.*, 2005, **401**, 426.
13 E. Reiser, S. Aust, V. Seebacher, A. Reinthaller, H. V. Mersi, R. Schwameis, S. Polterauer, C. Grimm and S. Helmy-Bader, *Eur. J. Obstet. Gynecol. Reprod. Biol.*, 2019, **239**, 16.
14 Y. Urano, M. Sakabe, N. Kosaka, M. Ogawa, M. Mitsunaga, D. Asanuma, M. Kamiya, M. R. Young, T. Nagano, P. L. Choyke and H. Kobayashi, *Sci. Transl. Med.*, 2011, **3**(110), 110.
15 Z. Thiel and P. Rivera-Fuentes, *Angew. Chem., Int. Ed.*, 2019, **58**, 11474.
16 Q. Zhang, S. S. Li, C. X. Fu, Y. Z. Xiao, P. Zhang and C. F. Ding, *J. Mater. Chem. B*, 2019, **7**(3), 443.
17 K. Li, Y. F. Lyu, Y. Huang, S. Xu, H. W. Liu, L. L. Chen, T. B. Ren, M. Y. Xiong, S. Y. Huan, L. Yuan, X. B. Zhang and W. H. Tan, *Proc. Natl. Acad. Sci. USA*, 2021, **118**(8), e2018033118.
18 J. G. Lin, D. Y. Gao, S. J. Wang, G. C. Lv, X. T. Wang, C. M. Lu, Y. Peng and L. Qiu, *J. Am. Chem. Soc.*, 2022, **144**, 7667.
19 B. B. Hu, N. Song, Y. W. Cao, M. M. Li, X. Liu, Z. F. Zhou, L. Q. Shi and Z. L. Yu, *J. Am. Chem. Soc.*, 2021, **143**(34), 13854.
20 Z. J. Qin, T. B. Ren, H. J. Zhou, X. X. Zhang, L. He, Z. Li, X. B. Zhang and L. Yuan, *Angew. Chem., Int. Ed.*, 2022, **61**(19), e202201541.
21 X. Wang, P. Li, Q. Ding, C. C. Wu, W. Zhang and B. Tang, *J. Am. Chem. Soc.*, 2019, **141**(5), 2061.
22 H. D. Li, Q. C. Yao, F. Xu, Y. Q. Li, D. Kim, J. Chung, G. Baek, X. F. Wu, P. F. Hillman, E. Y. Lee, H. Y. Ge, J. L. Fan, J. Y. Wang, S. J. Nam, X. J. Peng and J. Yoon, *Angew. Chem., Int. Ed.*, 2020, **59**(25), 10186.
23 T. Liu, J. Ning, B. Wang, B. Dong, S. Li, X. G. Tian, Z. L. Yu, Y. L. Peng, C. Wang, X. Y. Zhao, X. K. Huo, C. P. Sun, J. N. Cui, L. Feng and X. C. Ma, *Anal. Chem.*, 2018, **90**(6), 3965.
24 H. Y. Peng, T. Wang, G. R. Li, J. Huang and Q. Yuan, *Anal. Chem.*, 2022, **94**(2), 1070.
25 W. Li, S. L. Yin, X. Y. Gong, W. Xu, R. H. Yang, Y. C. Wan, L. Yuan and X. B. Zhang, *Chem. Commun.*, 2020, **56**, 1349.
26 S. J. Pan, S. Y. Jang, S. S. Liew, J. Q. Fu, D. Y. Wang, J. S. Lee and S. Q. Yao, *Angew. Chem., Int. Ed.*, 2018, **57**(2), 579.
27 X. Z. Chai, H. H. Han, A. C. Sedgwick, N. Li, Y. Zang, T. D. James, J. J. Zhang, X. L. Hu, Y. Yu, Y. Li, Y. Wang, J. Li, X. P. He and H. Tian, *J. Am. Chem. Soc.*, 2020, **142**(42), 18005.
28 L. K. B. Tam, J. C. H. Chu, L. He, C. X. Yang, K. C. Han, P. C. K. Cheung, D. K. P. Ng and P. C. Lo, *J. Am. Chem. Soc.*, 2023, **145**(13), 7361.
29 H. W. Liu, K. Li, X. X. Hu, L. M. Zhu, Q. M. Rong, Y. C. Liu, X. B. Zhang, J. Hasserodt, F. L. Qu and W. H. Tan, *Angew. Chem., Int. Ed.*, 2017, **56**(39), 11655.
30 Y. Y. Chen, H. Jiang, T. T. Hao, N. Zhang, N. Zhang, M. Y. Li, X. Y. Wang, X. X. Wang, W. Wei and J. Zhao, *Chem. Biomed. Imaging*, 2023, **1**(7), 590.
31 D. V. D. Gracht, R. J. Rowland, V. Roig-Zamboni, M. J. Ferraz, M. Louwerse, P. P. Geurink, J. M. F. G. Aerts, G. Sulzenbacher, G. J. Davies, H. S. Overkleeft and M. Artola, *Chem. Sci.*, 2023, **14**, 9136.
32 S. W. Chen, Y. Yin, X. Z. Pang, C. K. Wang, L. Wang, J. Q. Wang, J. F. Jia, X. X. Liu, S. H. Xu and X. L. Luo, *Chem. Sci.*, 2024, **15**, 566.
33 M. K. Goshisht, N. Tripathi, G. K. Patra and M. Chaskar, *Chem. Sci.*, 2023, **14**, 5842.
34 W. Hu, T. T. Qiang, C. C. Li, L. F. Ren, F. Cheng, B. S. Wang, M. L. Li, X. J. Song and T. D James, *Chem. Sci.*, 2022, **13**, 11140.
35 H. D. Li, Y. Q. Li, Q. C. Yao, J. L. Fan, W. Sun, S. Long, S. Kun, J. J. Du, J. Y. Wang and X. J. Peng, *Chem. Sci.*, 2019, **10**(6), 1619.
36 B. Ezekiel, *J. Biophot.*, 2008, **1**(3), 230.
37 A. Q. Zhong, Q. Fu, D. F. Huang, C. Wang, J. P. Zhu, S. Zhang and H. L. Jiang, *Optik*, 2023, **295**, 171512.
38 M. A. Steves and K. L. Knappenberger, *Chem. Biomed. Imaging*, 2023, **1**(1), 91.
39 A. Elbendary, M. Valdebran, K. Parikh and D. K. Elston, *Am. J. Dermatopathol.*, 2016, **38**(8), 593.
40 D. A. Hirth, A. J. Singer, R. A. F. Clark and S. A. McClain, *Wound Repair Regen.*, 2012, **20**(6), 918.
41 S. Gupta, R. Aggarwal, V. Gupta, R. Vij, N. Tyagi and A. Misra, *J. Histotechnol.*, 2017, **40**(2), 46.
42 J. M. Dubach, E. Kim, K. Yang, M. Cuccarese, R. J. Giedt, L. G. Meimetis, C. Vinegoni and R. Weissleder, *Nat. Chem. Biol.*, 2017, **13**(2), 168.
43 H. M. Kim, B. R. Kim, H. J. Choo, Y. G. Ko, S. J. Jeon, C. H. Kim, T. Joo and B. R. Cho, *ChemBioChem*, 2008, **9**, 2830.
44 R. W. Horobin, *Color. Technol.*, 2014, **130**(3), 155.

© 2024 The Author(s). Published by the Royal Society of Chemistry